Matrix Graphite Material Models in Pebbles and Compacts for Bison

30 September 2021

Technical Report

Aysenur Toptan[1], Wen Jiang[1], Stephen R. Novascone[1], and Jason D. Hales[1]

[1]Idaho National Laboratory

INL Idaho National Laboratory

Matrix Graphite Material Models in Pebbles and Compacts for Bison

Technical Report

Aysenur Toptan[1], Wen Jiang[1], Stephen R. Novascone[1], and Jason D. Hales[1]

[1]Idaho National Laboratory

30 September 2021

Idaho National Laboratory
Computational Mechanics and Materials Department
Idaho Falls, Idaho 83415

http://www.inl.gov

Abstract

The cores and reflectors in high-temperature gas-cooled reactors (HTGRs) are made of graphite materials, with the graphite acting as a moderator, a fuel host matrix, or the foundation for various structural components. This study aims to survey the models in the literature for graphite materials being used as host matrices in pebble/fuel compacts and to implement those surveyed models into Bison to conduct an early assessment of graphite's thermo-mechanical response under various reactor conditions. In this study, thermal (e.g., thermal conductivity, and specific heat capacity) and mechanical (e.g., elastic properties, thermal expansion, irradiation-induced dimensional changes, and irradiation-induced creep) material models for various graphite grades (e.g., H-451, IG-110, G-348, 2020, A3-3, and A3-27) are incorporated into Bison. Two benchmark problems are then exercised utilizing these new graphite-related capabilities: (1) modeling an Advanced Gas Reactor (AGR)-2 fuel compact, and (2) modeling the debonding of a particle-matrix interface.

DECLARATION OF COMPETING INTEREST

The authors declare that they have no known competing financial interests or personal relationships that could appear to have influenced the work reported in this technical report.

ORCID

Aysenur Toptan   ⓘ   orcid.org/0000-0003-4250-6336
Jason D. Hales   ⓘ   orcid.org/0000-0003-0836-0476
Stephen R. Novascone   ⓘ   orcid.org/0000-0002-3938-4326
Wen Jiang   ⓘ   orcid.org/0000-0001-6978-9159

CONTENTS

AD	automatic differentiation
AGR	Advanced Gas Reactor
ANL	Argonne National Laboratory
BAF	Bacon anisotropy factor
CTE	coefficient of thermal expansion
CZM	cohesive zone model
DOE	U.S. Department of Energy
D-EMT	differential effective medium theory
EFPD	effective full power days
FIMA	fissions per initial metal atom
HTGR	high-temperature gas-cooled reactor
IAEA	International Atomic Energy Agency
INL	Idaho National Laboratory
INDC	International Nuclear Data Committee
IPyC	inner pyrolytic carbon (PyC)
JAEA	Japan Atomic Energy Agency
MC	Monte Carlo
MOOSE	Multiphysics Object-Oriented Simulation Environment
NASA	National Aeronautics and Space Administration
NEA	Nuclear Energy Agency
NEAMS	Nuclear Energy Advanced Modeling and Simulation
NGKB	Nuclear Graphite Knowledge Base
NRC	U.S. Nuclear Regulatory Commission
OECD	Organisation for Economic Co-operation and Development
OPyC	outer PyC
PyC	pyrolytic carbon
SiC	silicon carbide
TRISO	tri-structural isotropic
3-D	three-dimensional

I. INTRODUCTION

The U.S. Department of Energy (DOE)'s Nuclear Energy Advanced Modeling and Simulation (NEAMS) program has focused on the development of predictive capabilities, using computational methods for the analysis and design of advanced reactor and fuel cycle systems. For several years, the NEAMS program has been supporting further development of Bison in the area of tri-structural isotropic (TRISO) modeling, in cooperation with the nuclear industry at large. Until now, engineering-scale modeling efforts in Bison [1] have focused on the thermo-mechanical properties of the TRISO particle and its constituent layers [2, 3, 4, 5, 6]. Extensive study has also been devoted to the code in order to compute the homogenized response of the graphite matrix (containing TRISO particles) thermal conductivity [7]. In this study, we aim to survey graphite material models widely used in HTGRs and then implement them into Bison, as well as perform benchmark examples using these models in order to conduct an early assessment of the needed material and/or physical models for future studies.

The cores and reflectors in high-temperature gas-cooled reactors (HTGRs) are made of graphite materials, with the graphite acting as a moderator; a fuel host matrix; a structural component to provide channels for the fuel, coolant gas, and control rods; a thermal and neutron shielding component; and a heat sink/conduction path during transients [8, 9, 10]. Our focus in this study is to investigate graphite grades used as a fuel host matrix containing TRISO particles. A TRISO fuel particle consists of a fuel kernel (made of UO_2, UCO, or UN) surrounded by a buffer and three coating layers: (1) an inner layer of high-strength PyC, referred to as inner PyC (IPyC); (2) a layer of silicon carbide (SiC); and (3) an outer layer of PyC, referred to as outer PyC (OPyC). These particles are embedded in a spherical or cylindrical graphite matrix, and this ensemble is referred to as a *fuel element*. Spherical fuel elements are often referred to as *pebbles*, while cylindrical fuel elements are referred to as *compacts*.

This report is organized as follows. The thermo-mechanical properties of each graphite grade (see Table I) are categorized into two main clusters, based on their categorization in Bison. Section II covers the thermal properties (e.g., thermal conductivity and specific heat capacity). Section III covers the mechanical properties (e.g., thermal expansion, elastic constants, irradiation-induced dimensional changes, and irradiation-induced creep). Section IV provides two benchmark problems (e.g., modeling of a fuel compact and particle-matrix debonding) in which the aforementioned material properties are utilized. Section V concludes this report by discussing the results and future work.

TABLE I. List of graphite grades investigated in this study.

Grade	Description
A3-3, A3-27	These grades are both produced via isostatic cold molding. Both graphites are heat-treated (at 1800 and 1950°C) during fabrication to improve their corrosion resistance. The main difference between A3-3 and A3-27 is the binder type: *"A3-3 has a thermoplastic (non-hardening resin) binder whereas A3-27 has a duroplastic (hardening) resin binder"* [11].
G-348	This grade is a product of Tokai Carbon USA [12]. It is formed via cold hydrostatic pressure molding, resulting in a (ultra) fine grain, high-density graphite. The material properties of this graphite are considered isotropic [13].
H-451	This historical grade, a product of the U.S. [14], was used as an HTGR fuel element and reflector [15]. The material properties of this graphite are considered anisotropic or nearly isotropic. It is formed via extrusion, with a maximum grain size of 500 μm. Its coke type is petroleum, and its density is 1960 kg/m³.
IG-110	This grade, a product of Japan, acts as a fuel host matrix. The material properties of this graphite are considered isotropic. This graphite is formed via isostatic molding, with a maximum grain size of 20 μm. The coke type is petroleum, and its density is 1780 kg/m³ [14].
2020	This grade is often used as the reference material for permanent side reflectors and central reflector column support blocks [15, 16]. It is isostatically molded and fine-grained in the form of either large rectangular or cylindrical blocks.

II. THERMAL PROPERTIES

The thermal properties of graphite addressed in this section cover thermal conductivity (Section II-A) and specific heat capacity (Section II-B).

A. Thermal Conductivity

Bison offers four graphite modeling options for computing the thermal conductivity of various graphite types, namely H-451 (Section II-A1), 2020 (Section II-A2), A3-3 and A3-27 (Section II-A3). In total, six models are available in the code to account for the effects of heat treatments on the thermal conductivity of A3-3 and A3-27 graphites.

Figure 1 compares the thermal conductivities of the aforementioned graphite grades under unirradiated conditions. The model for grade H-451 graphite yields significantly larger thermal conductivity predictions compared to the models for the other graphite grades. Both A3-3 and A3-27 graphites are heat treated during fabrication at one of two different temperatures (1800 or 1950°C). The heat-treated grades generate larger thermal conductivity predictions (10–20 W/m-K) than their untreated equivalents.
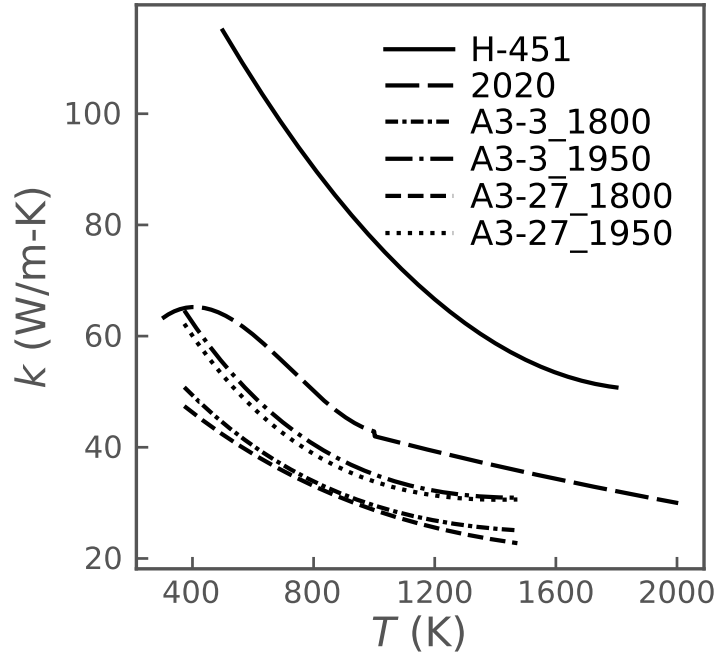
Fig. 1. Unirradiated thermal conductivity of graphite grades H-451[a], 2020[b], A3-3[c], and A3-27[c].
[a] **The model is considered valid over a temperature range of 500–1800 K.**
[b] **The model is considered valid over a temperature range of 300–2000 K.**
[c] **The A3-3 and A3-27 graphite grades were heat treated at 1800 and 1950°C during fabrication. The models are valid over a temperature range of 100–1200°C.**

Neutron fluence degrades thermal conductivity. The details of each thermal conductivity model for irradiated conditions are provided in the following sections. Note that the model predictions in the code are limited to their applicability ranges.

1) Grade H-451 graphite

Figure 2 shows the thermal conductivity of grade H-451 graphite as a function of neutron fluence and temperature. Empirical models are given at different neutron fluence values for the thermal conductivity as a function of temperature. To compute the thermal conductivity for a fluence of interest, interpolation is performed. Note that this model is considered valid over a temperature range of [500 K, 1800 K], and for neutron fluences of up to 8.0×10^{25} n/m^2 [16].
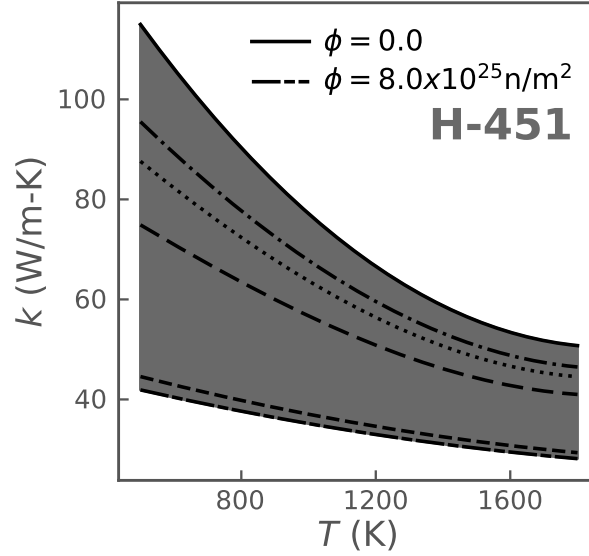
Fig. 2. Thermal conductivity of grade H-451 graphite [16] as a function of neutron fluence and temperature. The lines (from top to bottom) correspond to 0.0 (unirradiated), 0.2, 0.5, 1.0, 3.0, and 8.0×10^{25} n/m^2. Mathematical formulations for temperature-dependent thermal conductivity at various neutron fluence values are tabulated below.

Fluence (10^{25} n/m^2)	Thermal conductivity k (W/m-K)	Applicability
0.0	$k = 3.28248 \times 10^{-5}T_K^2 - 1.24890 \times 10^{-1}T_K + 169.2145$	500–1800 K
0.2	$k = 2.63319 \times 10^{-9}T_K^3 + 1.34998 \times 10^{-5}T_K^2 - 8.03309 \times 10^{-2}T_K + 131.991$	500–1800 K
0.5	$k = 3.60774 \times 10^{-9}T_K^3 + 6.45202 \times 10^{-6}T_K^2 - 6.38157 \times 10^{-2}T_K + 117.459$	500–1800 K
1.0	$k = 4.47613 \times 10^{-9}T_K^3 - 1.86131 \times 10^{-6}T_K^2 - 4.14540 \times 10^{-2}T_K + 95.5394$	500–1800 K
3.0	$k = 4.19346 \times 10^{-6}T_K^2 - 2.13523 \times 10^{-2}T_K + 54.1993$	500–1800 K
8.0	$k = 3.63529 \times 10^{-6}T_K^2 - 1.89383 \times 10^{-2}T_K + 50.4684$	500–1800 K

2) Grade 2020 graphite

Figure 3 shows the thermal conductivity of nuclear grade 2020 graphite as a function of neutron fluence and temperature. Empirical models are given at different neutron fluence values for thermal conductivity as a function of temperature. To compute the thermal conductivity for a fluence of interest, interpolation is performed. Note that

this model is considered valid over a temperature range of [300 K, 2000 K] and for neutron fluences of up to 20.0×10^{22} n/m^2 [16].
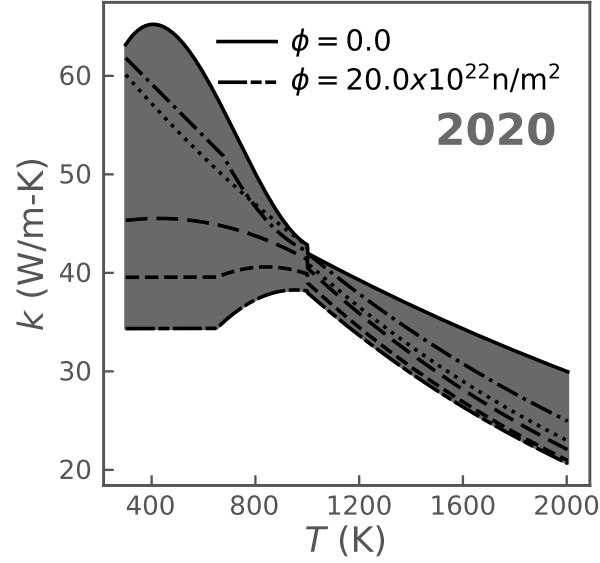
Fig. 3. Thermal conductivity of grade 2020 graphite [16] as a function of neutron fluence and temperature. The lines (from top to bottom) correspond to 0.0 (unirradiated), 0.4, 1.0, 4.0, 10.0, and 20.0×10^{22} n/m^2. Mathematical formulations for temperature-dependent thermal conductivity at various neutron fluence values are tabulated below.

Fluence (10^{22} n/m^2)	Thermal conductivity k (W/m-K)	Applicability
0.0	$k = 1.71039 \times 10^{-7}T_K^3 - 3.73458 \times 10^{-4}T_K^2 + 0.218725T_K + 26.5411$	300–1000 K
	$k = 58.800 \exp\left(-3.365 \times 10^{-4}T_K\right)$	1000–2000 K
0.4	$k = -0.0263158T_K + 69.71052632$	300–673 K
	$k = 5.89227 \times 10^{-5}T_K^2 - 0.128522T_K + 111.808$	673–1000 K
	$k = 70.560 \exp\left(-5.188 \times 10^{-4}T_K\right)$	1000–2000 K
1.0	$k = 7.53255 \times 10^{-6}T_K^2 - 3.46161 \times 10^{-2}T_K + 69.8153$	300–1000 K
	$k = 73.087 \exp\left(-5.781 \times 10^{-4}T_K\right)$	1000–2000 K
4.0	$k = -1.26995 \times 10^{-5}T_K^2 + 1.08450 \times 10^{-2}T_K + 43.2150$	300–1000 K
	$k = 74.219 \exp\left(-6.057 \times 10^{-4}T_K\right)$	1000–2000 K
10.0	$k = 39.55224$	300–650 K
	$k = -2.87164 \times 10^{-5}T_K^2 + 4.83551 \times 10^{-2}T_K + 20.2541$	650–1000 K
	$k = 72.429 \exp\left(-6.190 \times 10^{-4}T_K\right)$	1000–2000 K
20.0	$k = 34.34069$	300–650 K
	$k = -4.29785 \times 10^{-5}T_K^2 + 8.18658 \times 10^{-2}T_K - 0.713659$	650–1000 K
	$k = 69.758 \exp\left(-6.075 \times 10^{-4}T_K\right)$	1000–2000 K

3) Grade A3-3 and A3-27 graphite

The main difference between the A3-3 and A3-27 graphite grades is the binder type: *"A3-3 has a thermoplastic (non-hardening resin) binder whereas A3-27 has a duroplastic (hardening) resin binder"* [11]. The thermal conductivity of the unirradiated matrix depends on the nature of the matrix material and the temperature of the final heat treatment during fabrication [11]. During fabrication, both graphite grades were heat treated at one of two different temperatures (i.e., 1800 or 1950°C) to enhance their corrosion resistance. Here, we provide the thermal conductivities of A3-3 and A3-27 heat treated at 1800 and 1950°C. These models are hereafter referred to as A3-3_1800, A3-3_1950, A3-27_1800, and A3-27_1950. The correlation is given as a function of fast fluence, with a neutron energy threshold of E > 0.18 MeV [17, 11].

Hence, the thermal conductivity of the graphite, k_{graphite}, is:

$$k_{\text{graphite}} = k_{\text{unirr}} \kappa_\phi \kappa_\rho \tag{1a}$$

with

$$k_{\text{unirr}} = k_{100} \left[1 - \alpha \left(T_C - 100 \right) \exp \left(-\delta T_C \right) \right] \tag{1b}$$

$$\kappa_\phi = 1.0 - (0.94 - 0.604 t_C) \left\{ 1 - \exp \left(-\left[2.96 - 1.955 t_C \right] \frac{\phi}{1.52} \right) \right\} - \left(0.043 t_C - 0.008 t_C^8 \right) \frac{\phi}{1.52} \tag{1c}$$

$$\kappa_\rho = \frac{\rho}{\rho_0} \tag{1d}$$

where: k_{unirr} = the thermal conductivity of the unirradiated matrix material (see Equation 1b),

$\quad\quad\quad \kappa_\phi$ = a correction for irradiation damage (see Equation 1c),

$\quad\quad\quad \kappa_\rho$ = a correction for densities other than that of the reference material (see Equation 1d),

$\quad\quad\quad k_{100}$ = the thermal conductivity of non-porous material at 100°C (W/m-K),

$\quad\quad\quad T_C$ = the irradiation temperature (°C),

$\quad\quad\quad t_C$ = $T_C/1000$, the reduced temperature (°C),

$\quad\quad\quad \alpha, \delta$ = the empirical coefficients (see Table II),

$\quad\quad\quad \phi$ = the fast neutron fluence (10^{25} n/m^2, E > 0.18 MeV),

$\quad\quad\quad \rho$ = the density (kg/m^3), and

$\quad\quad\quad \rho_0$ = 1700 kg/m^3, the reference density.

Figure 4 plots the evolution graphite thermal conductivity as a function of temperature and fast neutron fluence for the A3-3 and A3-27 graphites—computed according the models provided in [11] (see Equation 1).

TABLE II. Coefficients for the unirradiated thermal conductivity of grade A3-3 and A3-27 graphites [11].

Graphite grade	k_{100} (W/m-K)	α	δ
A3-3_1800	50.8	1.1810×10^{-3}	7.8453×10^{-4}
A3-3_1950	64.6	1.4079×10^{-3}	9.0739×10^{-4}
A3-27_1800	47.4	9.7556×10^{-4}	6.0360×10^{-4}
A3-27_1950	62.2	1.4621×10^{-3}	9.6050×10^{-4}
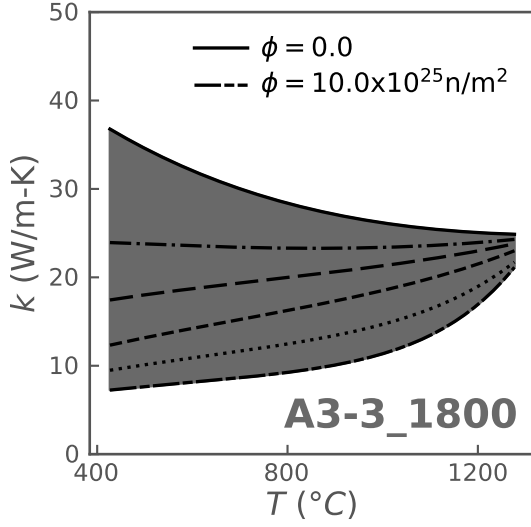
(a) A3-3 heat treated at 1800°C
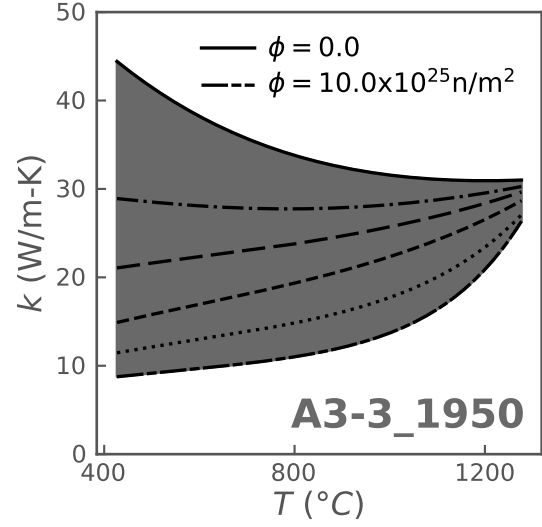
(b) A3-3 heat treated at 1950°C
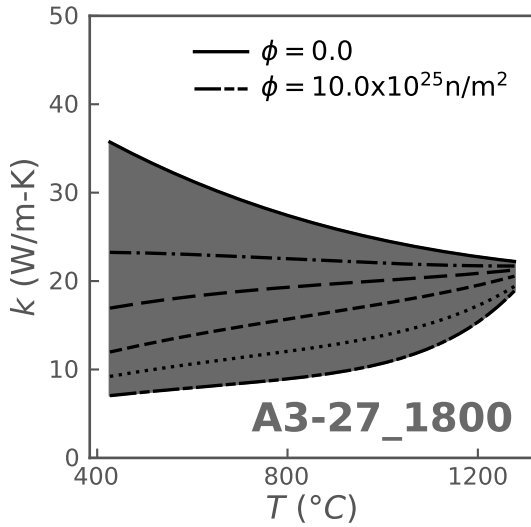
(c) A3-27 heat treated at 1800°C
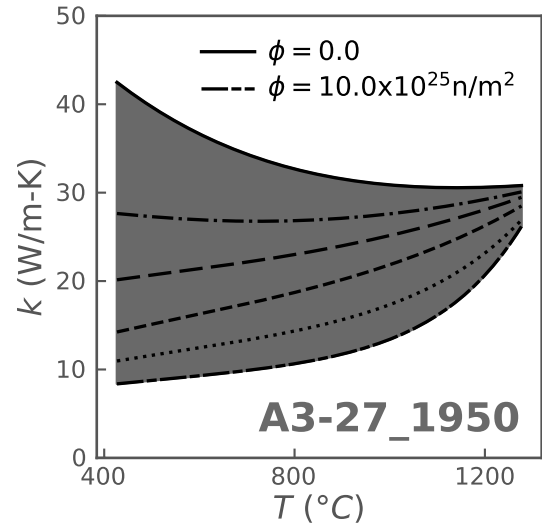
(d) A3-27 heat treated at 1950°C

Fig. 4. Changes in graphite thermal conductivity as a function of temperature and fast neutron fluence for the A3-3 and A3-27 graphites [11] with heat treatments at 1800 and 1950°C. The lines (from top to bottom) correspond to 0.0 (unirradiated), 0.5, 1.0, 2.0, 5.0, and 10.0×10^{25} n/m^2. The mathematical formulations are provided in Eqs. 1–1d.

B. Specific Heat Capacity

Bison offers two modeling options for computing the specific heat capacity of various graphite types. These options apply to carbon brick (Section II-B1) and grade H-451 (Section II-B2). The latter is considered valid for nuclear grade 2020 graphite, as per [16]. Figure 5 compares the specific heat capacities of the aforementioned graphite grades as a function of temperature. The model predictions are limited to their applicability ranges. The modeling options are detailed in the following sections.
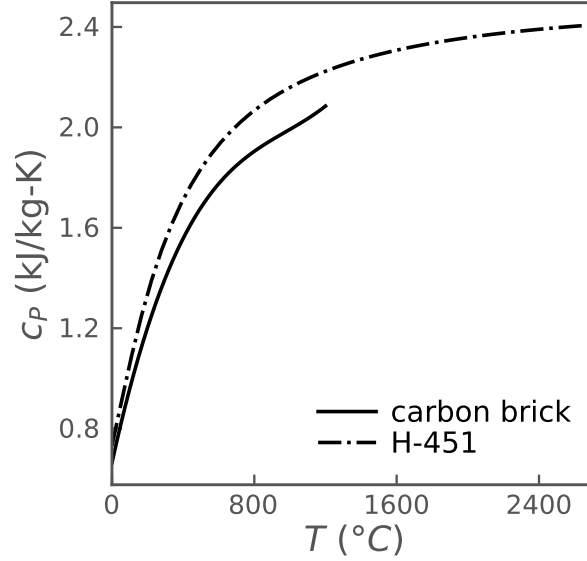
Fig. 5. Specific heat capacity of carbon brick[a] and H-451 graphite[b] as a function of temperature.
[a] **The model (Equation 2) is considered valid at up to 1200°C. The density is assumed to be 1700 kg/m³ here.**
[b] **The model (Equation 3) is considered valid over a temperature range of 250–3000 K.**

1) Carbon brick

The specific heat capacity of carbon brick is expressed in [18] as Equation 2. This model is considered valid at up to 1200°C [17] and is the default model option in the code [19]. Figure 5 shows the specific heat capacity of carbon brick as a function of temperature. For temperatures above 1200°C, the heat capacity is set to the heat capacity value of 1200°C.

$$c_P = \frac{1.75 \times 10^6}{\rho}\left(0.645 + 3.14\left[\frac{T_C}{1000}\right] - 2.809\left[\frac{T_C}{1000}\right]^2 + 0.959\left[\frac{T_C}{1000}\right]^3\right) \qquad (2)$$

where: T_C = the temperature (°C), and
ρ = the density (kg/m³).

2) Grade H-451 graphite

The specific heat capacity of grade H-451 graphite is expressed by [20] as Equation 3. This model is considered valid over the temperature range [250 K, 3000 K] (see Figure 5).

$$c_P = 4184\left(0.54212 - 2.42667 \times 10^{-6}T_K - \frac{90.2725}{T_K} - \frac{43449.3}{T_K^2} + \frac{1.59309 \times 10^7}{T_K^3} - \frac{1.43688 \times 10^9}{T_K^4}\right) \qquad (3)$$

where: T_K = the temperature (K).

Listing 1. Example Bison code syntax for the graphite and graphite matrix thermal properties [19].

```
[Materials]
  ...
  [matrix_thermal_props]
    type = GraphiteMatrixThermal
    graphite_grade = 'A3_27_1800'
    packing_fraction = 0.0
    specific_heat_scale_factor = 1.0
    etc_model = DEMT
    thermal_conductivity_scale_factor = 1.0
    temperature = temp
  []
  ...
[]
```

Example Bison code syntax

The `GraphiteMatrixThermal` model computes the thermal conductivity and specific heat capacity of various graphite grades and graphite-TRISO matrix compositions. To compute the thermal properties of a graphite grade, the packing fraction must be set to zero (i.e., `packing_fraction = 0.0`). To compute the thermal properties of a graphite matrix containing TRISO particles, homogenization is applied to the thermal conductivity for a non-zero packing fraction when `etc_model` is assigned to any selected homogenization model. The default homogenization model is the differential effective medium theory (D-EMT), based on the study by [7]. The different graphite grades available in the code (e.g., A3-3_1800, A3-3_1950, A3-27_1800, A3-27_1950, H-451, and 2020) are selected via the input parameter `graphite_grade` (see Listing 1). The default model option is A3-3_1800 [19].

The specific heat capacity of carbon brick (the default modeling option in the code) is calculated using the `GraphiteMatrixThermal` model with `graphite_grade = A3_3_1800, A3_3_1950, A3_27_1800,` or `A3_27_1950`. For a graphite-TRISO matrix, a volumetric average of the specific heat capacities is computed and assigned to the matrix specific heat capacity.

An AD version is also available by adding the prefix `AD` to the name of the `type` parameter (i.e., `type = GraphiteMatrixThermal`).

III. MECHANICAL PROPERTIES

The mechanical properties of the various graphite grades addressed in this section cover elastic constants (Section III-A), thermal expansion (Section III-B), irradiation-induced dimensional changes (Section III-C), and irradiation-induced creep (Section III-D).

A. Elastic Properties

Bison offers two modeling options for computing the elastic constants for graphite H-451 (Section III-A1) and 2020 (Section III-A2). The following sections detail the mathematical formulations of each model.

1) Grade H-451 graphite

In terms of the fractional change, κ_p (as a function of fast neutron fluence), and the irradiation temperature, irradiation affects the moduli as follows [15]:

$$\frac{E_1}{E_{1o}} = \frac{E_3}{E_{3o}} = \left(1.0 + 1.5 \times 10^{-4} \left[T_C - 21\right]\right) \kappa_p \tag{4}$$

where: E_1, E_3 = the elastic modulus of irradiated graphite at room temperature,
E_{1o}, E_{3o} = the elastic modulus of unirradiated graphite at room temperature,
T_C = the temperature (°C), and
κ_p = the fractional change due to the fast neutron fluence and temperature (see Figure 6).

The Poisson's ratio is considered constant under irradiation conditions (i.e., $\nu = 0.12$). Note that room temperature is considered to be 21°C in [15]. The mean values of the transversely isotropic elastic constants at room temperature, neglecting the effect of spatial distribution in this study, are given by [15] as:

$$E_{1o} = 7.35\,\text{GPa}$$
$$E_{3o} = 8.31\,\text{GPa} \tag{5}$$
$$\nu = 0.12$$

This model is considered valid over the temperature range [673 K, 1473 K], and for fast neutron fluences up to 8.0×10^{25} n/m².

2) Grade 2020 graphite

Irradiation affects the elastic moduli through the fractional increase, p (see Figure 7), which is a function of fast neutron fluence, per:

$$\frac{E_1}{E_{1o}} = \frac{E_3}{E_{3o}} = 1 + p \tag{6}$$

where: E_1, E_3 = the elastic modulus of irradiated graphite at room temperature,
E_{1o}, E_{3o} = the elastic modulus of unirradiated graphite at room temperature, and
p = the fractional release in the elastic modulus (see Figure 7).

The temperature dependency is given as:

$$E_1 = E_{1o} - 9.94 \times 10^{-4} \left(T_C - 21\right) + 3.09 \times 10^{-6} \left(T_C - 21\right)^2 \tag{7a}$$

$$E_3 = E_{3o} - 9.94 \times 10^{-4} \left(T_C - 21\right) + 3.09 \times 10^{-6} \left(T_C - 21\right)^2 \tag{7b}$$

where: T_C = the temperature (°C).

Fig. 6. Fractional increase in the elastic modulus as a function of irradiation conditions for grade H-451 graphite. The numerical values are tabulated below:

Fluence $(10^{25}$ n/m$^2)$	Irradiation temperature				Fluence $(10^{25}$ n/m$^2)$	Irradiation temperature			
	673 K	873 K	1173 K	1473 K		673 K	873 K	1173 K	1473 K
0.00	0.000	0.000	0.000	0.000	4.25	1.210	1.012	0.906	0.715
0.25	0.830	0.680	0.540	0.520	4.50	1.228	1.020	0.959	0.727
0.50	0.905	0.768	0.638	0.620	4.75	1.243	1.028	1.010	0.732
0.75	0.950	0.816	0.686	0.666	5.00	1.260	1.034	1.060	0.743
1.00	0.981	0.853	0.714	0.685	5.25	1.274	1.040	1.113	0.752
1.25	1.008	0.880	0.732	0.690	5.50	1.290	1.047	1.168	0.767
1.50	1.028	0.904	0.750	0.690	5.75	1.306	1.053	1.220	0.781
1.75	1.048	0.920	0.757	0.690	6.00	1.322	1.059	1.272	0.798
2.00	1.065	0.935	0.767	0.690	6.25	1.338	1.065	1.324	0.815
2.25	1.080	0.948	0.770	0.690	6.50	1.354	1.071	1.376	0.834
2.50	1.098	0.955	0.774	0.690	6.75	1.370	1.078	1.428	0.859
2.75	1.113	0.965	0.780	0.690	7.00	1.386	1.084	1.480	0.885
3.00	1.130	0.975	0.787	0.690	7.25	1.402	1.090	1.532	0.912
3.25	1.145	0.984	0.793	0.692	7.50	1.418	1.096	1.584	0.948
3.50	1.163	0.990	0.808	0.700	7.75	1.434	1.102	1.636	0.984
3.75	1.174	1.000	0.823	0.705	8.00	1.452	1.106	1.690	1.030
4.00	1.193	1.008	0.852	0.710					

The Poisson's ratio is considered constant during irradiation conditions (i.e., $\nu = 0.15$). Note that room temperature is considered to be 21°C in [15]. Transversely isotropic linear elastic constants at the room temperature are given by [15] as:

$$E_{1o} = 9.5\,\text{GPa}$$
$$E_{3o} = 8.9\,\text{GPa} \tag{8}$$
$$\nu = 0.15$$

This model is considered valid at temperatures up to 1100°C and fast neutron fluences up to 10.0×10^{22} n/m^2.
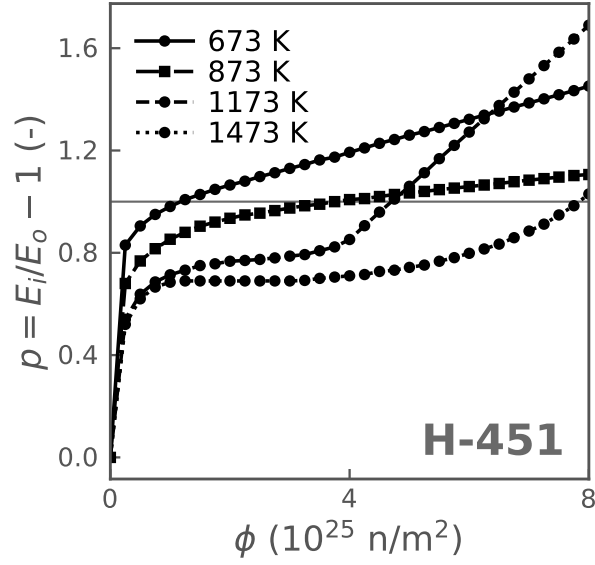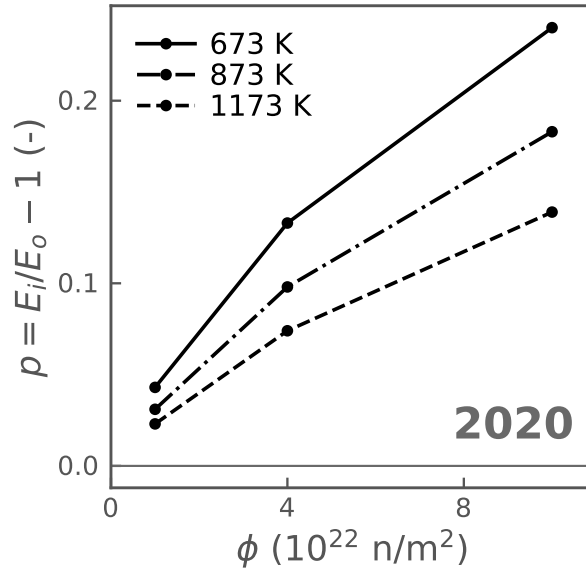

Fig. 7. Fractional increase in the elastic modulus as a function of irradiation conditions for grade 2020 graphite. The numerical values are tabulated below:

Fluence	Irradiation temperature		
(10^{22} n/m^2)	673 K	873 K	1173 K
1.0	0.043	0.031	0.023
4.0	0.133	0.098	0.074
10.0	0.240	0.183	0.139

Example Bison code syntax

The `GraphiteGradeElasticityTensor` model computes the elastic properties of various graphite grades. Two options are available in the code for the graphite grades H-451 and 2020. The creep calculation typically uses a return mapping algorithm to determine the necessary increment of creep strain to return the stress state to the yield surface. The radial return mapping algorithm implemented in the Multiphysics Object-Oriented Simulation Environment (MOOSE) [21] assumes an isotropic shear modulus that is incompatible with a transversely isotropic elasticity tensor; therefore, we recommend an isotropic elasticity tensor with a Young's modulus of 7.83 GPa and

a Poisson's ratio of 0.12 for graphite H-451, and with a Young's modulus of 9.2 GPa and a Poisson's ratio of 0.15 for graphite IG-110. This feature will be incorporated into the code at some point in the near future.

B. Thermal Expansion

Bison offers three modeling options for computing the thermal expansion eigenstrain for graphite types H-451 (Section III-B1), IG-110 (Section III-B2), and G-348 (Section III-B3). The following sections detail the mathematical formulations of each model.

1) Grade H-451 graphite

The thermal expansion of H-451 graphite during neutron irradiation is computed according to [15]. The mean coefficient of thermal expansion (CTE) for unirradiated H-451 at 20–500°C, $\bar{\alpha}_{(20-500)}$, is 4.09×10^{-6} K^{-1} (or °C^{-1}) in the axial direction and 4.65×10^{-6} K^{-1} in the radial direction. In this study, we assign $\bar{\alpha}_{(20-500)}$ to 4.37×10^{-6} K^{-1} (i.e., the mean of both values) for use in both directions. Hence, the mean CTE can be computed for H-451 graphite as per Equation 9. Figure 8 shows the change in the mean CTE of grade H-451 graphite as a function of fast neutron fluence and temperature.

$$\bar{\alpha}_{(20-T)} = \bar{\alpha}_{(20-500)} f_\alpha(T, \phi) \tag{9a}$$

with the fractional change in thermal expansivity due to irradiation, $f_\alpha(T, \phi)$, calculated as:

$$\begin{aligned} f_\alpha(T, \phi) =&\, 1.0 + \left(0.27830 - 4.2734 \times 10^{-4} T_C + 1.7815 \times 10^{-7} T_C^2\right) \phi \\ &- 2.0664 \times 10^{-2} \phi^2 + 1.3601 \times 10^{-3} \phi^3 \end{aligned} \tag{9b}$$

where: $T_C =$ the irradiation temperature (°C), and
ϕ = the fast neutron fluence (10^{25} n/m^2).
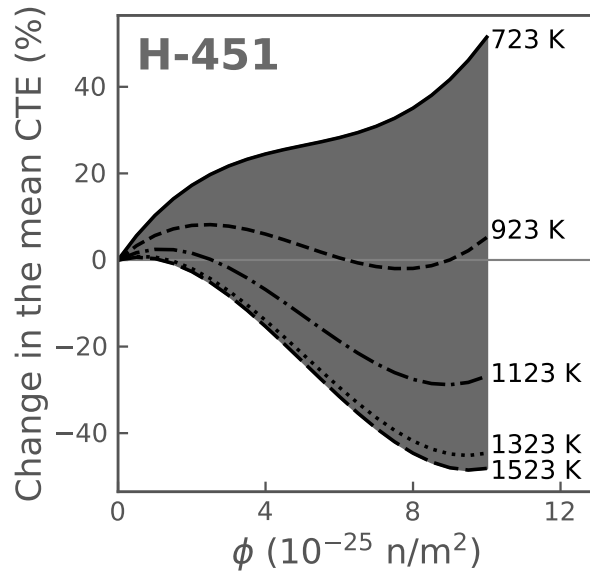
Fig. 8. **Change in the mean CTE of grade H-451 graphite as a function of neutron fluence at various irradiation temperatures (from top to bottom): 723, 923, 1123, 1323, and 1523 K.**

2) Grade IG-110 graphite

The mean CTE, $\alpha_{(20-T)}$ (K^{-1}), is expressed by [22] as Equation 10. This model is considered valid over a temperature range of 100–1500°C. Figure 9 shows the change in the mean CTE of grade IG-110 graphite as a function of temperature.

$$\bar{\alpha}_{(20-T)} = \bar{\alpha}_{(20-400)} f_{\alpha}(T) \tag{10a}$$

with the fractional change in thermal expansivity due to the temperature, $f_{\alpha}(T)$, as:

$$f_{\alpha}(T) = 0.853157 + 4.26564 \times 10^{-4} T_C - 1.42849 \times 10^{-7} T_C^2 \tag{10b}$$

where: $\alpha_{(20-400)} = 4.06 \times 10^{-6}$ K^{-1}, and
T_C = the temperature (°C).
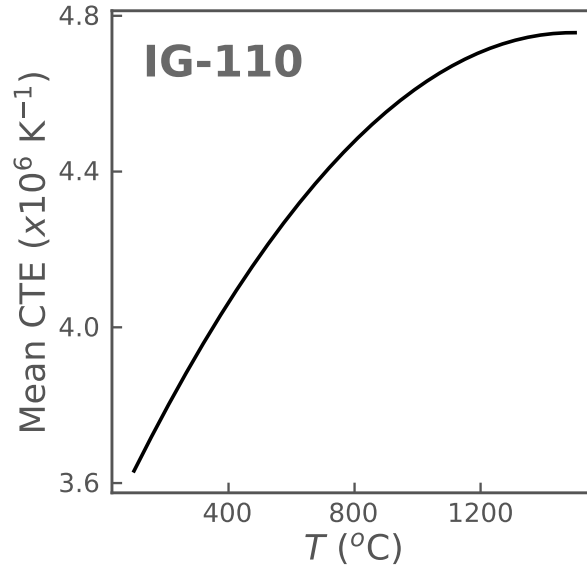
Fig. 9. Change in the mean CTE of grade IG-110 graphite as a function of temperature. This model is considered valid over a temperature range of 100–1500°C.

3) Grade G-348 graphite

The mean CTE, $\alpha_{(20-T)}$ (K^{-1}), of grade G-348 graphite is expressed by [13] as Equation 11. This model is considered valid at temperatures up to 1000°C. Figure 10 shows the change in the mean CTE of grade G-348 graphite as a function of temperature.

$$\bar{\alpha}_{(20-T)} = 4.812 \times 10^{-6} + 1.145 \times 10^{-9} (T_C + 30) \tag{11}$$

where: T_C = the temperature (°C).

Example Bison code syntax

The `GraphiteGradeThermalExpansionEigenstrain` model computes eigenstrain due to thermal expansion by using a function that describes the mean thermal expansion of the graphite grade as a function of
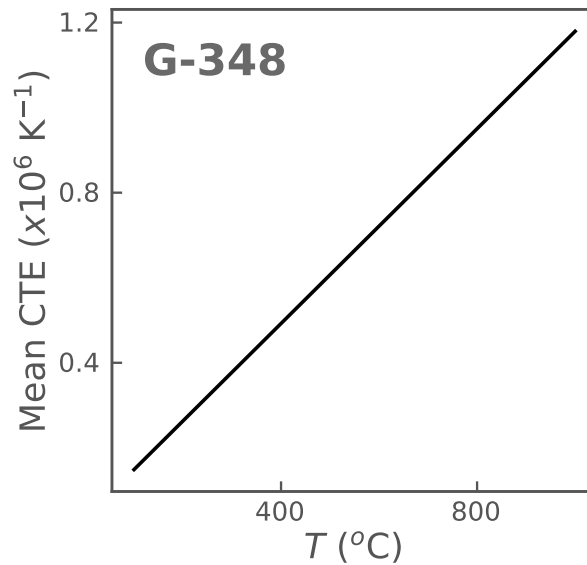
Fig. 10. Change in the mean CTE of grade G-348 graphite as a function of temperature. This model is considered valid at temperatures up to 1000°C.

Listing 2. Example Bison code syntax for the use of GraphiteGradeThermalExpansionEigenstrain.

```
[Materials]
  ...
  [thermal_expansion]
    type = GraphiteGradeThermalExpansionEigenstrain
    eigenstrain_name = thermal_expansion
    graphite_grade = H_451
    stress_free_temperature = 293.15
    flux_conversion_factor = 0.8
    temperature = temp
    thermal_expansion_scale_factor = 1.0
  []
  ...
[]
```

temperature and/or fast neutron fluence. Different options are available in the code for the graphite grades (e.g., G-348, H-451, and IG-110), and grade selection is performed via `graphite_grade` (see Listing 2).

An AD version is also available by adding the prefix `AD` to the name for the `type` parameter (i.e., `type = ADGraphiteGradeThermalExpansionEigenstrain`).

C. Irradiation-Induced Dimensional Change

Bison has two modeling options for computing the irradiation-induced dimensional change: grade H-451 graphite (Section III-C1) and grade IG-110 graphite (Section III-C2). The following sections detail the mathematical formulations of each model.

1) Grade H-451 graphite

The irradiation-induced dimensional change, ε^I (%), of grade H-451 graphite is expressed in [15] as Equation 12. This model is considered valid over a temperature range of 623–1573 K and for fast neutron fluences up to 10×10^{25} n/m^2.

$$
\begin{aligned}
\varepsilon^I = {} & \left(c_1 + c_2 T_C + c_3 T_C^2 + c_4 T_C^3 + c_5 T_C^4\right)\phi \\
& + \left(c_6 + c_7 T_C + c_8 T_C^2 + c_9 T_C^3 + c_{10} T_C^4 + c_{16} T_C^5\right)\phi^2 \\
& + \left(c_{11} + c_{12} T_C + c_{13} T_C^2 + c_{14} T_C^3 + c_{15} T_C^4 + c_{17} T_C^5 + c_{18} T_C^6\right)\phi^3
\end{aligned}
\tag{12}
$$

where: ϕ = the fast neutron fluence (10^{25} n/m^2),
T_C = the irradiation temperature (°C), and
c_i = the empirical coefficients for each orientation (Figure 11).
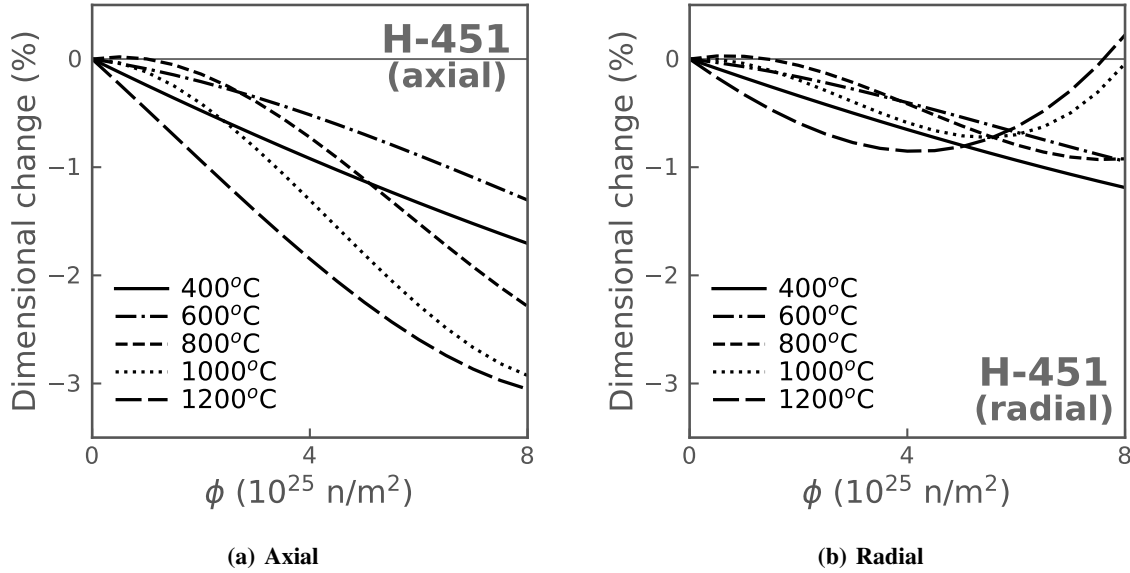
(a) Axial

(b) Radial

Fig. 11. Irradiation-induced dimensional changes of grade H-451 graphite as a function of temperature, and neutron fluence in the (a) axial and (b) radial directions. Empirical coefficients used in Equation 12 for dimensional changes of H-451 graphite [15] are tabulated below.

i	c_i (axial)	c_i (radial)	i	c_i (axial)	c_i (radial)
1	1.11617	1.15132	10	0.20435×10^{-10}	0.14233×10^{-10}
2	-0.92197×10^{-2}	-0.82968×10^{-2}	11	-0.59274×10^{-2}	0.13110×10^{-1}
3	0.20463×10^{-4}	0.17060×10^{-4}	12	-0.65404×10^{-5}	-0.18768×10^{-3}
4	-0.16458×10^{-7}	-0.12645×10^{-7}	13	0.32751×10^{-6}	0.10199×10^{-5}
5	0.40809×10^{-11}	0.27657×10^{-11}	14	-0.13449×10^{-8}	-0.27004×10^{-8}
6	0.64947	0.39177	15	0.22245×10^{-11}	0.36498×10^{-11}
7	-0.56929×10^{-2}	-0.36540×10^{-2}	16	-0.51973×10^{-14}	-0.35768×10^{-14}
8	0.18972×10^{-4}	0.12750×10^{-4}	17	-0.16038×10^{-14}	-0.23579×10^{-14}
9	-0.29277×10^{-7}	-0.20230×10^{-7}	18	0.41756×10^{-18}	0.57329×10^{-18}

2) Grade IG-110 graphite

The irradiation-induced dimensional change, ε^I (%), of grade IG-110 graphite is expressed in [14] by [23] as:

$$\varepsilon^I = a_1\phi^2 + a_2\phi \tag{13}$$

where: $a_1, a_2 =$ the temperature-dependent empirical coefficients (see Figure 12), and
ϕ = the fast neutron fluence (10^{26} n/m^2).
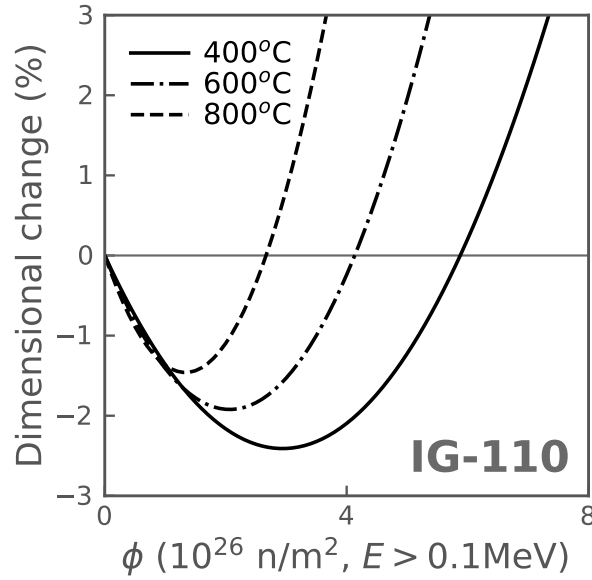
Fig. 12. Irradiation-induced dimensional changes of grade IG-110 graphite as a function of neutron fluence at various irradiation temperatures. The empirical coefficients used in Equation 13 for dimensional changes of grade IG-110 graphite [14, 23] are tabulated below.

	400°C	600°C	800°C
a_1	0.279	0.450	0.821
a_2	-1.64	-1.86	-2.19

Example Bison code syntax

The `GraphiteGradeIrradiationEigenstrain` model computes irradiation-induced dimensional changes for graphite grades H-451 (anistoropic) and IG-110 (isotropic). The selection is performed via `graphite_grade`.

An AD version is also available by adding the prefix `AD` to the name of the `type` parameter (i.e., `type = GraphiteGradeIrradiationEigenstrain`).

D. Irradiation-Induced Creep

Bison offers a modeling option for computing irradiation-induced creep in grade H-451 graphite (Section III-D1). The following section details the mathematical formulation of the model.

Listing 3. Example Bison code syntax for the use of GraphiteGradeIrradiationEigenstrain.

```
[Materials]
  ...
  [graphite_irrad_strain]
    type = GraphiteGradeIrradiationEigenstrain
    temperature = temperature
    graphite_grade = H_451 # IG_110
    flux_conversion_factor = 0.85
    eigenstrain_name = irrad_strain
  []
  ...
[]
```

Listing 4. Example Bison code syntax for the use of GraphiteGradeCreepUpdate in conjunction with ComputeMultipleInelasticStress.

```
[Materials]
  ...
  [GraphiteGrade_creep]
    type = GraphiteGradeCreepUpdate
    flux_conversion_factor = 0.85
    graphite_grade = H_451
    temperature = temp
    creep_scale_factor = 1.0
    outputs = all
  []
  [stress]
    type = ComputeMultipleInelasticStress
    tangent_operator = elastic
    inelastic_models = 'GraphiteGrade_creep'
  []
  ...
[]
```

1) Grade H-451 graphite

Irradiation-induced creep strain, ε_{cr} (-), in H-451 graphite is expressed by [24] as Equation 14. This model is considered valid over a temperature range of 773–1473 K and for neutron fluences up to 10×10^{25} n/m^2.

$$
\begin{aligned}
\varepsilon_{cr} = 4.16 \times 10^{-5} \sigma \left[1 - \exp\left(-5 \times 10^{-24} \phi\right)\right] \exp\left(1.27 \times 10^{-3} T_K\right) \\
+ 6.2 \times 10^{-30} \sigma \phi \exp\left(7.48 \times 10^{-4} T_K\right)
\end{aligned}
\tag{14}
$$

where: σ = the applied stress (MPa),
ϕ = the fast neutron fluence (n/m^2), and
T_K = the temperature (K).

Example Bison code syntax

The `GraphiteGradeCreepUpdate` model computes irradiation-induced creep for grade H-451 graphite. This material must be run in conjunction with `ComputeMultipleInelasticStress`. The selection is performed via `graphite_grade` (see Listing 4).

An AD version is also available by adding the prefix `AD` to the name of the `type` parameter (i.e., `type = GraphiteGradeCreepUpdate`).

IV. DEMONSTRATION EXAMPLES

The aim of the demonstration examples is to identify and prioritize the needed models for conducting an early assessment of graphite's thermo-mechanical response under various reactor conditions. This section covers two examples exercising the newly implemented material models for TRISO fuel elements using Bison:

1) Modeling of an AGR-2 compact in Section IV-A, which explores the thermo-mechanical behavior at the fuel element level; and

2) Modeling of particle-matrix debonding in Section IV-B, which explores the thermo-mechanical behavior at the particle level.

Fuel specifications and irradiation conditions for both benchmark problems are tabulated in Table III and Table IV, respectively. In both demonstration problems, grade H-451 graphite models are used, mainly due to the availability of these material models. In those applications, the aforementioned material models for thermal conductivity, specific heat, thermal expansion, irradiation eigenstrain, and creep (see Section II and Section III) are employed. Note that MOOSE's creep solver does not work with transversely isotropic elasticity at present. Therefore, an isotropic elasticity tensor with a Young's modulus of 7.83 GPa and a Poisson's ratio of 0.12 for graphite H-451 are used in the simulations.

TABLE III. Fuel specifications in benchmark problems.

Category	Parameter	Nominal values ± 1 standard deviation
Fuel characteristics	^{235}U enrichment	15.5 wt.%
	Carbon/uranium (atomic ratio)	0.4
	Oxygen/uranium (atomic ratio)	1.5
Particle geometry	Kernel diameter	425 ± 10 μm
	Buffer thickness	100 ± 10 μm
	IPyC/OPyC thickness	40 ± 3 μm
	SiC thickness	35 ± 2 μm
	Particle asphericity (SiC aspect ratio)	1.04
Fuel properties	Kernel density	11.0 g/cm^3
	Kernel theoretical density	11.4 g/cm^3
	Buffer density	1.05 g/cm^3
	Buffer theoretical density	2.25 g/cm^3
	IPyC density	1.90 ± 0.02 g/cm^3
	OPyC density	1.90 ± 0.02 g/cm^3
	IPyC/OPyC BAF	1.05 ± 0.005

TABLE IV. Irradiation conditions for benchmark problems.

Parameter	Value
Effective full power days (EFPD)	500.0
Burnup	13.5% FIMA
Fast neutron fluence	5.0×10^{25} n/m^2 ($E >$0.18 MeV)
Irradiation temperature	700.0°C

A. AGR-2 Compact Modeling

The AGR-2 compact is a cylindrical fuel element containing roughly 4000 TRISO particle fuels. Figure 13 shows the three-dimensional (3-D) computational domain, with the randomly distributed TRISO particles hosted in a H-451 graphite matrix. The height and diameter of the fuel compact are 25 and 12 mm, respectively. The TRISO fuel properties are listed in Table III. A recent Bison capability is used to couple TRISO particles that are randomly generated from a Monte Carlo (MC) simulation to the host matrix so that the thermo-mechanical properties of the particles and the matrix are in simultaneous communication. For further details on the coupling approach, refer to [25]. The simulations are performed under the irradiation conditions listed in Table IV.
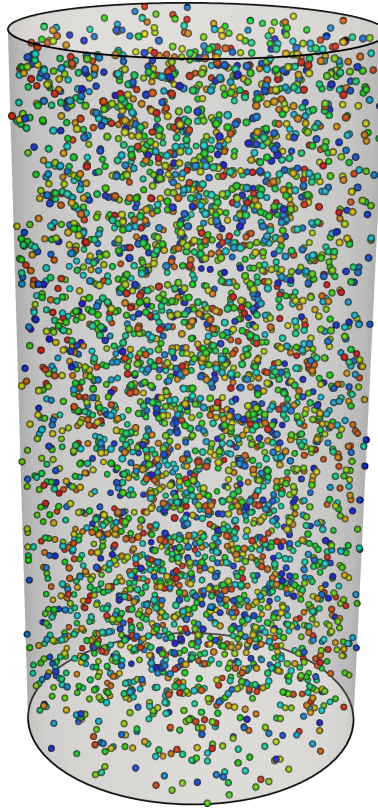
Fig. 13. Fuel compact containing 4000 TRISO particles randomly generated from an MC simulation. The particles are coupled to the host matrix by using a recent Bison capability so that the thermo-mechanical properties of each are in simultaneous communication.

Figure 14 shows the Bison predictions (at the end of irradiation) for temperature, effective creep strain, tangential stress, and radial stress. Higher temperatures are observed at the core of the fuel compact, which is 30 K hotter than at the compact exterior. The effective creep strain varies between 1.4×10^{-4} to approximately 6×10^{-4}. The fuel compact creeps the most at mid-height. While similar behavior is observed for the tangential stress at mid-height, higher tangential predictions are also observed at the top and bottom center of the compact. Lastly, the radial stress has its maximum values (around 2.0×10^6 Pa) at the top and bottom center of the compact. Overall, the simulation results seem reasonable. A more rigorous verification and validation study will be exercised in the future. As mentioned, isotropic elasticity is considered in this simulation, due to the lack of a creep solver option in

MOOSE for transversely isotropic elasticity constants. This might cause a slight difference in the thermo-mechanical response of the fuel compact.

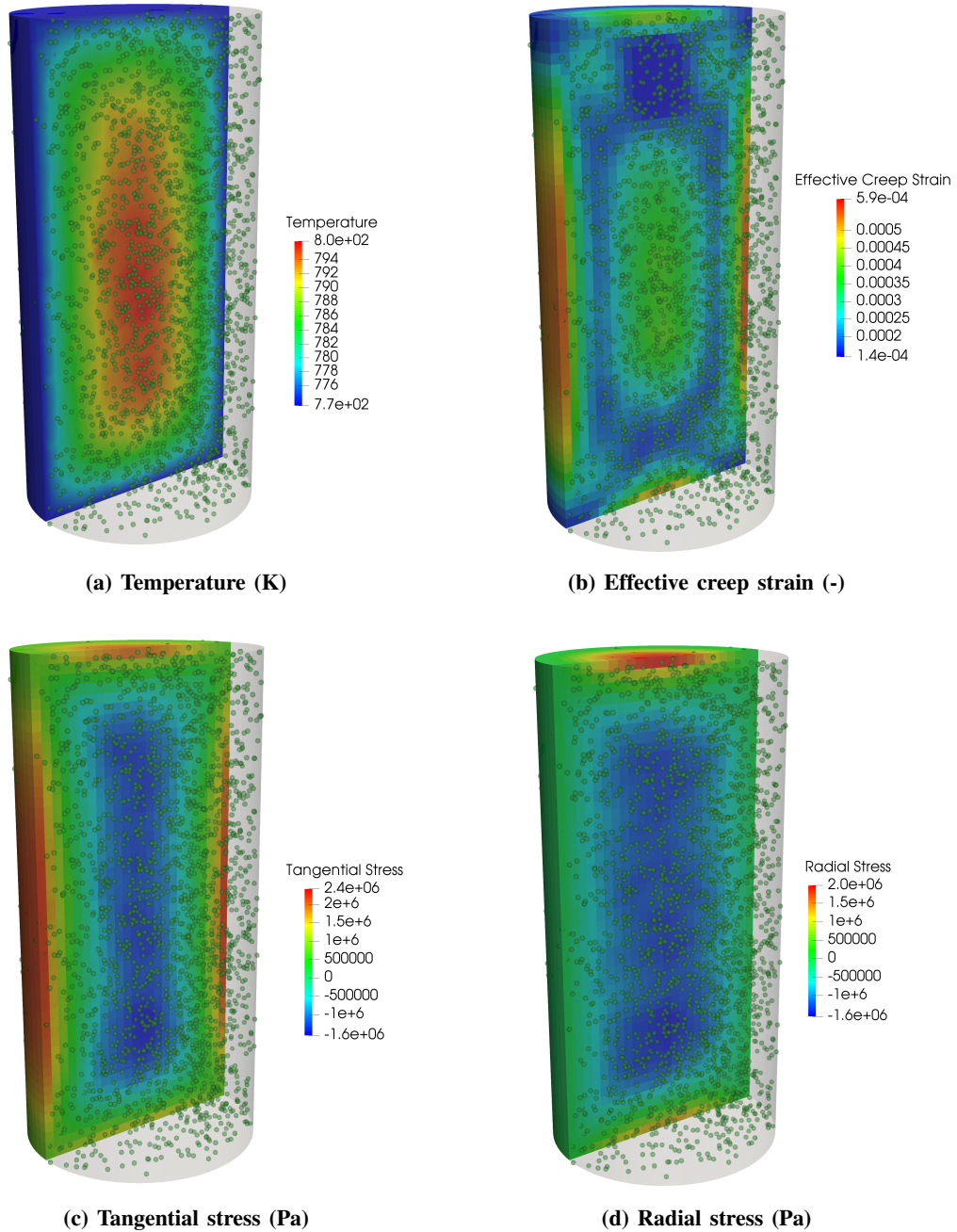(a) Temperature (K)

(b) Effective creep strain (-)

(c) Tangential stress (Pa)

(d) Radial stress (Pa)

Fig. 14. AGR-2 compact simulation results at the end of irradiation.

B. Particle-Matrix Debonding

In the second example, the particle-matrix debonding phenomenon is investigated. Debonding of the particle from the matrix is experimentally evident from the AGR experiments. Figure 15 shows the 3-D computational domain of a one-eighth symmetric model used in our analyses. A five-layer TRISO particle is considered, surrounded by grade H-451 graphite. The fuel specifications and irradiation conditions for this analysis are identical to those considered in the previous example. The TRISO particle is fully bonded to the graphite matrix at the beginning of the simulation. The stiffness of the material is expected to increase when the particles are fully bonded to the matrix.

The cohesive zone model (CZM) is used to simulate the debonding of the particle (i.e., the outermost—OPyC—layer of the TRISO particle) from the graphite matrix. The CZM is a well-known modeling approach in fracture mechanics, with the separation of the crack surfaces gradually forming through the crack tip (namely, the cohesive zone). This model is advantageous due to its accurate modeling of the behaviors of cracked and uncracked solids. The theoretical basis for the CZM can be found in [26]. Bond strength, a required simulation parameter in the CZM, is set to 8 MPa in our analyses.
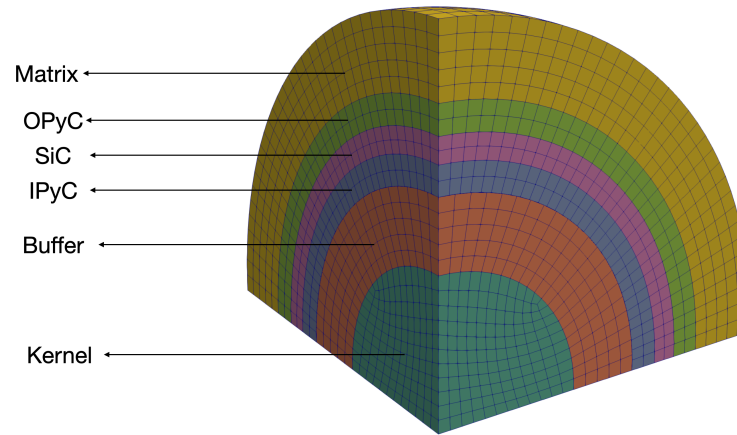
Fig. 15. Finite element model for a TRISO particle in a graphite matrix. A one-eighth symmetric, 3-D computational domain is considered in this analysis. The TRISO particle is fully bonded to the graphite matrix.

Figure 16 shows the tangential stresses during irradiation at various times. The TRISO particle is fully bonded to the matrix at the beginning of irradiation, as shown in Figure 15. The particle is still bonded to the matrix at $t = 24$ days (see Figure 16a). Debonding of the particle from the graphite matrix occurs at around $t = 92$ days (see Figure 16b). The gap size between the matrix and OPyC layer starts to increase due to the OPyC shrinkage (see Figure 16c). Then, it decreases as the matrix shrinks due to irradiation (see Figure 16d).

Although our primary focus in this analysis is on investigating particle-matrix debonding, there is also significant debonding of the buffer layer from the IPyC layer. The gap between the buffer layer and IPyC layer continues to increase with irradiation.
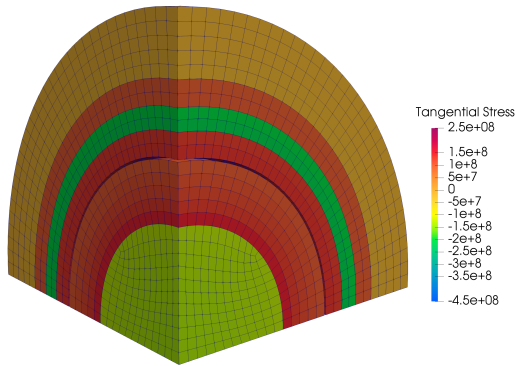
(a) t = 24 days
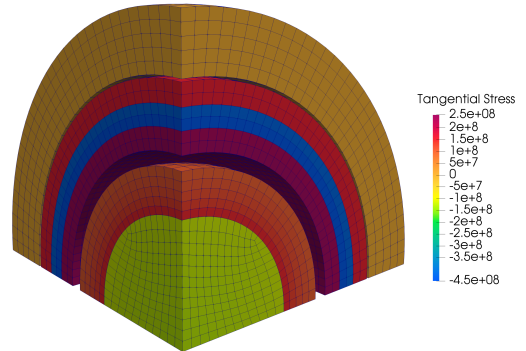
(b) t ≈ 92 days
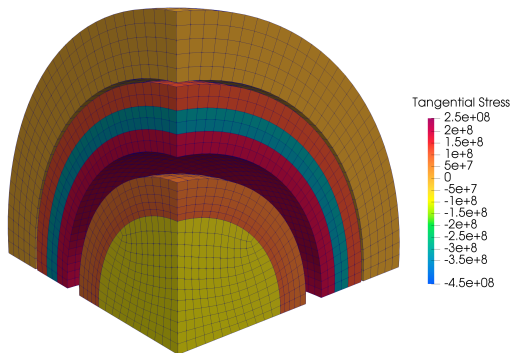
(c) t ≈ 192 days
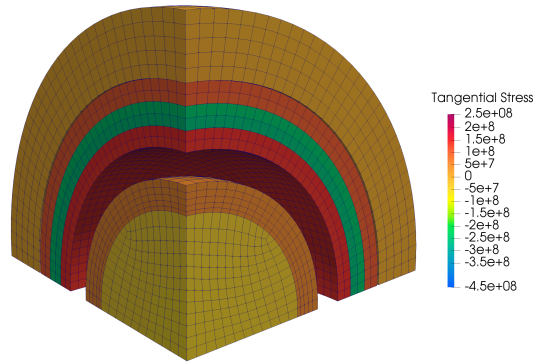
(d) t ≈ 485 days

Fig. 16. Tangential stress during irradiation for the particle-matrix debonding example (displacements are magnified 2x).

V. Conclusion

Up until now, modeling efforts in Bison have mainly focused on the thermo-mechanical response of the TRISO fuel particle and its constituent layers. In this study, our efforts focused on enhancing Bison's material modeling options for the various graphite grades used in the fuel host matrix, and exercising benchmark problems that utilize these new capabilities in order to identify needed material properties to conduct early assessment of the thermo-mechanical response of graphite.

Because the thermo-mechanical properties of graphite strongly depend on its resin binder type and manufacturing processes, individual material models may be subject to change—except as regards the homogenization methods, which have a more general applicability. Thus, we harvested from the literature the available material models for various graphite grades. Key physical properties identified by [10] are irradiation dimensional stability, strength, elastic moduli, thermal expansion coefficient, radiation creep, fracture behavior, and oxidation behavior. In this study, we surveyed and implemented material models into Bison that cover these identified models (except for fracture and oxidation behaviors). A summary of the thermal and mechanical models made available in Bison is tabulated in Table V. The models in this table are categorized as pertaining to either thermal or mechanical properties.

TABLE V. Summary of available thermal and mechanical material properties for various graphite grades in Bison. The newly added material models in this study are indicated in the last column of the table below.

Material Property (Bison material property name[‡])	Graphite grade	Ref.	This study
Thermal properties			
Specific heat capacity (GraphiteMatrixThermal)	Carbon brick[†]	[18]	[3]
	H-451	[20]	✓
	2020	[16]	✓
Thermal conductivity (GraphiteMatrixThermal)	A3-3-1800[†], -1950	[11]	[3]
	A3-27-1800, -1950	[11]	[3]
	H-451	[16]	✓
	2020	[16]	✓
Mechanical properties			
Elasticity[§] (GraphiteGradeElasticityTensor)	H-451	[15, 14]	✓
	2020	[14]	✓
Irradiation-induced creep (GraphiteGradeCreepUpdate)	H-451[†]	[24]	✓
Irradiation-induced dimensional change (GraphiteGradeIrradiationEigenstrain)	H-451[†]	[15]	✓
	IG-110	[14, 23]	✓
Thermal expansion (GraphiteGradeThermalExpansionEigenstrain)	H-451[†]	[15]	✓
	IG-110	[22]	✓
	G-348	[13]	✓

‡ The material property names in the code at present.

† The default modeling option in the code.

§ This material property requires a new elasticity tensor solver option in MOOSE for transversely isotropic elasticity constants.

The aforementioned material properties were utilized in two benchmark problems: (1) modeling an AGR-2 compact and (2) modeling particle-matrix debonding. In these benchmark problems, we explored the graphite's thermo-mechanical response at two different levels: the fuel element and the particle levels. In the first benchmark

problem, Bison's new capability was used to couple particles that were randomly generated from a MC simulation to the host matrix, enabling simultaneous communication between the properties of the particles and the matrix. In the second benchmark problem, the particle-matrix debonding phenomenon was investigated in a one-eighth symmetric, 3-D computational domain in which the TRISO particle was surrounded by H-451 graphite. Identical fuel specifications and irradiation conditions were applied to both benchmark problems.

This work establishes a strong basis for modeling graphite, and demonstrates advancement in Bison's modeling capabilities for particle-matrix debonding and mechanical interactions. In the future, this work can be expanded to include the following phenomena—based on observations made during the benchmark analyses—to accurately assess graphite performance:

- Many graphite grades are highly or nearly anisotropic. As mentioned, isotropic elasticity was assumed in this simulation, due to the present lack of an elasticity solver option in MOOSE for transversely isotropic conditions. Enhancing the solver capabilities for non-isotropic materials will enable more realistic modeling of the particle-graphite matrix behavior.

- Oxidation effects on the graphite mechanical properties were not accounted for in this study. Air/moisture oxidation likely occurs in most graphite-moderated reactors, resulting in property degradation. Several parameters are required for accurately modeling the oxidation behavior in graphite, including the kinetics of oxidation reactions and the local partial pressure of oxidizing species within the graphite [10]. To accurately assess graphite performance, it is important to include the oxidation effects on graphite mechanical properties.

- Grade H-451 graphite was chosen for the benchmark problems of this study, mainly due to the availability of material models found in the literature. This graphite is a historical grade and discontinued. For assessing the performance of commercial graphite, new material models must be developed, and more experimental evidence gathered to support the validity of each model. The International Atomic Energy Agency (IAEA) Nuclear Graphite Knowledge Base (NGKB) (see Appendix A) can be useful for developing new models, if required, as well as for validating the widely used models in the literature.

REFERENCES

[1] R. L. Williamson et al. "BISON: A flexible code for advanced simulation of the performance of multiple nuclear forms". In: *Nuclear Technology* 207.7 (2021), pp. 954–980. DOI: 10.1080/00295450.2020.1836940.

[2] J.D. Hales et al. "Multidimensional multiphysics simulation of TRISO particle fuel". In: *Journal of Nuclear Materials* 443.1 (Nov. 2013), pp. 531–543. DOI: 10.1016/j.jnucmat.2013.07.070.

[3] J. D. Hales et al. *BISON TRISO Modeling Advancements and Validation to AGR-1 Data*. PEMP Notable Outcome 1.1.C Completion Report INL/EXT-20-59368. Idaho Falls, ID United States: Idaho National Laboratory (INL), 2020. DOI: 10.2172/1711423. URL: https://www.osti.gov/biblio/1711423/.

[4] W. Jiang et al. "TRISO particle fuel performance modeling and failure analysis with BISON". In: *Journal of Nuclear Materials* 548 (May 2021), p. 152795. DOI: 10.1016/j.jnucmat.2021.152795.

[5] J. D. Hales et al. "Modeling fission product diffusion in TRISO fuel particles with BISON". In: *Journal of Nuclear Materials* 548 (May 2021), 152840:1–16. DOI: 10.1016/j.jnucmat.2021.152840.

[6] J. D. Hales et al. "Numerical evaluation of AGR-2 fission product release". In: *Journal of Nuclear Materials* (2021), p. 153325. DOI: 10.1016/j.jnucmat.2021.153325.

[7] A. Toptan et al. "FEA-aided investigation of the effective thermal conductivity in a medium with embedded spheres". In: *Nuclear Engineering and Design* 381 (Sept. 2021), p. 111355. DOI: 10.1016/j.nucengdes.2021.111355.

[8] B. J. Marsden. *Nuclear graphite for high temperature reactors*. Tech. rep. IAEA-TECDOC–1238. Vienna, Austria: IAEA, 2001. URL: https://inis.iaea.org/collection/NCLCollectionStore/_Public/32/047/32047840.pdf?r=1.

[9] X. Zhou et al. "Nuclear graphite for high temperature gas-cooled reactors". In: *New Carbon Materials* 32.3 (June 2017). DOI: 10.1016/S1872-5805(17)60116-1.

[10] T. Burchell. *HTGR Technology Course for the Nuclear Regulatory Commission, Module 9 Graphite*. Accessed: 19–Aug-2021. May 2010. URL: https://art.inl.gov/NGNP/Training%20Modules%20%20HTGR%20Fundamentals/Module%209%20-%20Graphite.pdf.

[11] R. Gontard and H. Nabielek. *Performance Evaluation of Modern HTR TRISO Fuels*. Tech. rep. HTA-1B-05/90. Forschungszentrums Juelich, July 1990.

[12] F. I. Valentín et al. "Study of Convection Heat Transfer in a Very High Temperature Reactor Flow Channel: Numerical and Experimental Results". In: *Nuclear Technology* 196.3 (2016), pp. 661–673. DOI: 10.13182/NT16-46.

[13] W. D. Swank et al. "Thermal Conductivity of G-348 Isostatic Graphite". In: *Nuclear Technology* 199.1 (2017), pp. 103–109. DOI: 10.1080/00295450.2017.1317530.

[14] S. Mohanty and S. Majumdar. *HTGR Graphite Core Component Stress Analysis Research Program - Task 1*. Technical Letter Report ANL-11/04. prepared for U.S. Nuclear Regulatory Commission (NRC). Argonne National Laboratory, Illinois (United States): Argonne National Laboratory (ANL), Sept. 2011. URL: https://www.nrc.gov/docs/ML1127/ML11276A009.pdf.

[15] F. H. Ho. *Graphite Design Handbook*. Tech. rep. DOE-HTGR-88111. General Atomics, 1991. URL: https://www.osti.gov/servlets/purl/714896.

[16] Nuclear Energy Agency (NEA) Nuclear Science Committee. *NEA Benchmark of the Modular High-Temperature Gas-Cooled Reactor-350 MW Core Design: Volumes I and II*. Tech. rep. NEA/NSC/R(2017)4. Organisation for Economic Co-operation and Development (OECD), Feb. 2018. URL: https://www.oecd.org/officialdocuments/publicdisplaydocumentpdf/?cote=NEA/NSC/R(2017)4&docLanguage=En.

[17] G. K. Miller, et al. *PARFUME Theory and Model Basis Report*. Tech. rep. INL/EXT-08-14497 (Rev.1). Idaho Falls, ID (United States): Idaho National Laboratory (INL), Sept. 2018. DOI: 10.2172/1471713. URL: https://www.osti.gov/biblio/1471713-parfume-theory-model-basis-report.

[18] International Atomic Energy Agency (IAEA). *Heat Transport and Afterheat Removal for Gas Cooled Reactors Under Accident Conditions*. Tech. rep. IAEA-TECDOC-1163. Vienna, Austria, 2000. URL: https://www-pub.iaea.org/MTCD/Publications/PDF/te_1163_prn.pdf.

[19] Bison Team, Computational Mechanics and Materials Department, Idaho National Laboratory (INL). *Bison: A Finite Element-Based Nuclear Fuel Performance Code*. https://mooseframework.inl.gov/bison/.

[20] A. T. D. Butland and R. J. Maddison. "The specific heat of graphite: An evaluation of measurements". In: *Journal of Nuclear Materials* 49.1 (Nov. 1973), pp. 45–56. DOI: 10.1016/0022-3115(73)90060-3.

[21] C. J. Permann et al. "MOOSE: Enabling massively parallel multiphysics simulation". In: *SoftwareX* 11 (2020), p. 100430. DOI: 10.1016/j.softx.2020.100430.

[22] D. K. L. Tsang et al. "Graphite thermal expansion relationship for different temperature ranges". In: *Carbon* 43.14 (Nov. 2005), pp. 2902–2906. DOI: 10.1016/j.carbon.2005.06.009.

[23] T. Shibata et al. *Draft of standard for graphite core components in high temperature gas-cooled reactor*. Tech. rep. JAEA Research 2009-042. Japan: Japan Atomic Energy Agency (JAEA), Jan. 2010. URL: https://www.osti.gov/etdeweb/biblio/21417319.

[24] G. B. Engle. *Assessment of Grade H-451 Graphite For Replaceable Fuel and Reflector Elements in HTGR*. Tech. rep. GA-A14690. General Atomic Company, Dec. 1977. DOI: 10.2172/5176415. URL: https://www.osti.gov/servlets/purl/5176415-FEFJpl/.

[25] W. Jiang et al. *Fission product transport in TRISO particles and pebbles*. Tech. rep. INL/EXT-21-63549. Idaho Falls, ID United States: Idaho National Laboratory (INL), 2021. DOI: 10.2172/1818294. URL: https://www.osti.gov/biblio/1818294.

[26] P. P. Camanho and C. G. Dávila. *Mixed-Mode Decohesion Finite Elements for the Simulation of Delamination in Composite Materials*. Tech. rep. NASA/TM-2002-211737. National Aeronautics and Space Administration (NASA), June 2002. URL: https://citeseerx.ist.psu.edu/viewdoc/download?doi=10.1.1.8.267&rep=rep1&type=pdf.

[27] M. Gladyshev, F. Reitsma, and T. Yasar. *International Atomic Energy Agency (IAEA) Nuclear Graphite Knowledge Base*. Nuclear Data Library (*Last update: Apr-2015*). Vienna, Austria. URL: https://www.iaea.org/resources/databases/iaea-nuclear-graphite-knowledge-base.

[28] F. Reitsma and N. C. Gallego. *Overview of IAEA Nuclear Graphite Knowledge Base (NGKB) (NGKB)*. International Nuclear Graphite Specialist Meeting (INGSM 2019). Sept. 2019.

[29] T. D. Burchell et al. *IAEA International database on irradiated nuclear graphite properties*. Tech. rep. INDC(NDS)-413. Vienna, Austria: International Nuclear Data Committee (INDC), International Atomic Energy Agency (IAEA), Feb. 2000. URL: https://inis.iaea.org/collection/NCLCollectionStore/_Public/31/014/31014441.pdf.

A. IAEA Nuclear Graphite Knowledge Database

The format of the *International Atomic Energy Agency (IAEA) Nuclear Graphite Knowledge Base (NGKB)* is shown in Table A.1. Experimental data exist for several graphite grades. The database represents a total of over 30,000 experimental data points.

TABLE A.1. IAEA Nuclear Graphite Database [27, 28, 29].

A	B	C	D	E	F	G	H	I	J	K	L
						SAMPLE CHARACTERISTICS					
Graphite Grade	Sample Number		Orientation	Manufacturer	Coke Source	Binder	Filler	Number of Impregnations	Impregnant	Forming Process	Graphitisation Temperature (°C)

M	N	O	P	Q	R	S	T	U	V	W	X
(con't)	Neutron	Irradiation	Irrad.	a Initial	a Final	c Initial	c Final	La Initial	La Final	Lc Initial	Lc Final
							CRYSTALLITE PARAMETERS				
Additional Information	Fluence (dpa)	Temp. (°C)	Experiment	$(10^{-10}$ m)	$(10^{-10}$ m)	$(10^{-10}$ m)	$(10^{-10}$ m)	$(10^{-10}$ m)	$(10^{-10}$ m)	$(10^{-10}$ m)	$(10^{-10}$ m)

Y	Z	AA	AB	AC	AD	AE	AF	AG	AH	AI	AJ
								ELASTIC PROPERTIES			
E-Modulus (Static)				G-Modulus (Static)				E (Dynamic)			
Initial E_0 (GPa)	Final E (GPa)	Final/Initial	E/E_0-1 (%)	Initial (GPa)	Final (GPa)	Final/Initial	Initial (GPa)	Final (GPa)	Final/Initial	E/E_0-1 (%)	Initial Freq. $(10^3$/s)

AK	AL	AM	AN	AO	AP	AQ	AR	AS	AT	AU	AV
						ELECTRICAL RESISTIVITY					
G (Dynamic)				Poisson's Ratio							
Final Freq. $(10^3$/s)	Initial (GPa)	Final (GPa)	Final/Initial	Initial	Final	Initial (Ohm*m*10^{-6})	Final (Ohm*m*10^{-6})	Final/Initial	Fractional Change (%)	Measuring Temperature (°C)	Initial $(10^6$/K)

AW	AX	AY	AZ	BA	BB	BC	BD	BE	BF	BG	BH
			THERMAL PROPERTIES								
Thermal Expansion Coefficient				Thermal Conductivity				Tensile			
Final $(10^{-6}$/K)	Temp Range (°C)	Final/Initial	Fract.Change (%)	Initial k_0 (W/m K)	Final k (W/m K)	k/k_0-1	Meas Temp (°C)	Initial (MPa)	Final (MPa)	Final/Initial	Initial (MPa)

BI	BJ	BK	BL	BM	BN	BO	BP	BQ	BR	BS	BT
STRENGTH						DIMENSIONAL CHANGES					
Compr.		Bending			Length			Diameter			Thickness
Final (MPa)	Final/Initial	Initial (MPa)	Final (MPa)	Final/Initial	Initial (mm)	Final (mm)	Change (%)	Initial (mm)	Final (mm)	Change (%)	1 (mm)

BU	BV	BW	BX	BY	BZ	CA	CB	CC	CD	CE	CF
				ACOUSTIC PROPERTIES				IRRADIATION CREEP			
(con't)		Volume		Sonic Velocity		Attenuation		Applied	Creep	Creep	
2 (mm)	Initial (cm^3)	Final (cm^3)	Change (%)	Initial (m/s)	Final (m/s)	Initial (db/mm)	Final (db/mm)	Stress (MPa)	Strain (%)	Coeff $(10^{-35}$m^2/Pa)	

CG	CH	CI	CJ	CK	CL	CM	CN	CO	CP	CQ	CR
STORED ENERGY			PORE VOLUME		DENSITY			OTHER PROPERTIES			
		Release	Open Porosity					Initial Mass	Final Mass	Mass Loss	
Total S (J/g)	dS/dt (J/(g*s))	Start Temp (°C)	Initial (%)	Final (%)	Initial (g/cm^3)	Final (g/cm^3)	Change (%)	(g)	(g)	(%)	Ordinal Number